Skyrmion physics in Bose-Einstein ferromagnets

U. Al Khawaja and H. T. C. Stoof
Institute for Theoretical Physics, University of Utrecht, Princetonplein 5,3584 CC Utrecht, The Netherlands
(Received 26 April 2001; published 19 September 2001)

We show that a ferromagnetic Bose-Einstein condensate has not only line-like vortex excitations, but in general, also allows for pointlike topological excitations, i.e., skyrmions. We discuss the thermodynamic stability and the dynamic properties of these skyrmions for both spin-1/2 and ferromagnetic spin-1 Bose gases.

DOI: 10.1103/PhysRevA.64.043612 PACS number(s): 03.75.Fi, 03.65.Db, 05.30.Jp, 32.80.Pj

I. INTRODUCTION

An understanding of quantum magnetism is important for a large number of phenomena in physics. Three well-known examples are high-temperature superconductivity, quantum phase transitions, and the quantum Hall effect. Moreover, it appears that magnetic properties are also very important in another area, namely, Bose-Einstein condensation in trapped atomic gases. This has come about because of two independent experimental developments. The first development is the realization of an optical trap for atoms, whose operation no longer requires the gas to be doubly spin polarized [1,2]. The second development is the creation of a two-component Bose-Einstein condensate [3], which by means of rf fields may be manipulated so as to make the two components essentially equivalent [4]. As a result, the behavior of both spin-1 and spin-1/2 Bose gases can now be experimentally explored in detail. Indeed, at present, already such diverse phenomena as domain walls [5], macroscopic quantum tunneling [6], Rabi oscillations, and vortices [7] have been observed.

Theoretically, the ground-state structure of these gases has recently been worked out by a number of authors [8–11] and also the first studies of the linelike vortex excitations have appeared [8,12,13]. However, an immediate question that comes to mind is whether the spin degrees of freedom allow for other topological excitations that do not have an analogy in the case of a single component or scalar Bose condensate. It is one of the aims of this paper to show that the answer to this question is, in general, affirmative. In particular, we show that a ferromagnetic Bose-Einstein condensate has so-called skyrmion excitations, which are nonsingular but nevertheless topologically nontrivial pointlike spin textures. Roughly speaking, the skyrmion is an excitation that can be created out of the ground state, in which all the spins are aligned, by reversing the average spin in a finite region of space. Skyrmions are also known from nuclear physics [14] and the quantum Hall effect [15], but to observe them in an atomic gas would be exciting, since in that case, a completely microscopic understanding of their behavior is possible. In nuclear physics and the quantum Hall effect this is not true because of the nonperturbative nature of QCD and the presence of impurities that obstruct the center-of-mass motion of the skyrmions, respectively. Having proven their existence, we then turn to the investigation of the precise texture, the energetic stability, and finally the dynamical behavior of skyrmions. Some of the results of this analysis we have already reported in previous communications [16], but here we try to give a much more complete and detailed picture of the skyrmion physics in spinor Bose-Einstein condensates.

With this in mind, we would like to mention that we recently have also considered 't Hooft–Polyakov monopoles [17] in an antiferromagnetic Bose-Einstein condensate [18]. These topological excitations are in fact singular skyrmions, but have quite different properties than the nonsingular skyrmions, which are the object of study in this paper. In particular, due to the singular nature of the spin texture of the 't Hooft–Polyakov monopole, the condensate density vanishes in the core and the monopole turns out to be thermodynamically stable. This is completely analogous to the case of a vortex in a scalar Bose-Einstein condensate. Both these features are not shared by the nonsingular skyrmions, which complicates the analysis considerably. The most important problem in this respect is that for a nonsingular skyrmion, the topology allows for a spin texture with an arbitrary intrinsic size. As a result, the stability of the skyrmion is now determined by energetic arguments and not by topological arguments, as in the case of the singular 't Hooft-Polyakov monopole.

The paper is organized as follows. In Sec. II, we use the symmetry properties of the order parameter of a spinor Bose-Einstein condensate to show that, quite generally, skyrmion excitations indeed exist in such a condensate. We then turn our attention to the ferromagnetic case and discuss some general properties of these topological excitations, especially the spin texture, the superfluid velocity profile, and also the density profile. In Sec. III, we investigate the energetic stability of the skyrmion and show that from a thermodynamic point of view they are always unstable and tend to decrease to microscopic sizes. As a result, we then consider the dynamical stability of the skyrmion and, in particular, determine the rate at which they collapse. We find that under certain conditions, this rate is actually much smaller than the decay rate of the condensate itself due to various inelastic processes. Therefore, the skyrmion may for all practical purposes, be considered as a (meta)stable excitation and we are justified to look in Sec. IV also at other important dynamic properties of the skyrmion such as the ''spin'' and the center-of-mass motion. Finally, we end in Sec. V by a summary and some conclusions.

II. SKYRMIONS AS TOPOLOGICAL EXCITATIONS

In this section, we discuss in detail the main static features of skyrmions. First of all, we show from the symmetry

of the order-parameter space of the spinor condensate, that from a topological point of view pointlike skyrmion excitations may indeed exist in both spin-1/2 and spin-1 Bose-Einstein condensates. Focusing then on the ferromagnetic case, we introduce a convenient parametrization of the skyrmion texture, which allows us to incorporate most easily the nontrivial winding number associated with the skyrmion. Next, we write down the energy functional for a ferromagnetic spinor condensate and, by substituting the above-mentioned parametrization, derive the corresponding Euler-Lagrange equations for the density profile and the spin texture of the skyrmion. Finally, to simplify the actual calculation of the skyrmion density profile and the spin texture, we propose a variational approach that automatically takes into account the desired overall features of the skyrmion texture.

A. Topological considerations

To find all possible topological excitations of a spinor condensate, we need to know the full symmetry of the macroscopic wave-function $\Psi(\mathbf{r}) \equiv \sqrt{n(\mathbf{r})}\zeta(\mathbf{r})$, where $n(\mathbf{r})$ is the total density of the gas, $\zeta(\mathbf{r})$ is a normalized spinor that determines the average local spin by means of $\langle \mathbf{S} \rangle(\mathbf{r}) = \zeta_a^*(\mathbf{r})\mathbf{S}_{ab}\zeta_b(\mathbf{r})$, and $\mathbf{S}$ are the usual spin matrices obeying the commutation relations $[S_\alpha, S_\beta] = i\epsilon_{\alpha\beta\gamma}S_\gamma$. Note that here, and in the following, summation over repeated indices is always implicitly implied. From the work of Ho [8], we know that in the case of spin-1 bosons we have to consider two possibilities, since the effective interaction between two spins can be either antiferromagnetic or ferromagnetic. In the antiferromagnetic case, the ground-state energy is minimized for $\langle \mathbf{S} \rangle(\mathbf{r}) = \mathbf{0}$, which implies that the parameter space for the spinor $\zeta(\mathbf{r})$ is only $U(1) \times S^2$ because we are free to choose both its overall phase and the spin quantization axis. In the ferromagnetic case, the energy is minimized for $|\langle \mathbf{S} \rangle(\mathbf{r})| = 1$ and the parameter space corresponds to the full rotation group SO(3). Using the same arguments, we find that for spin-1/2 bosons, the order-parameter space of the ground state is always equivalent to SU(2) [19].

What do these results tell us about the possible topological excitations [20,21]? For linelike defects or vortices, we can assume $\zeta(\mathbf{r})$ to be independent of one direction and the spinor represents a mapping from a two-dimensional plane into the order-parameter space. If the vortex is singular, this will be visible on the boundary of the two-dimensional plane and we need to investigate the properties of a continuous mapping from a circle S^1 into the order-parameter space G, i.e., of the first homotopy group $\pi_1(G)$. Since $\pi_1(\mathrm{SU}(2)) = \pi_1(\mathrm{SO}(3)) = Z_2$ and $\pi_1(\mathrm{U}(1) \times S^2) = Z$, we conclude that a spin-1/2 and a ferromagnetic spin-1 condensate may have only vortices with a winding number equal to one, whereas an antiferromagnetic spin-1 condensate may have vortices with winding numbers that are an arbitrary integer. Physically, this means that by traversing the boundary of the plane, the spinor may wind around the order parameter at most once or an arbitrary number of times, respectively. This conclusion is identical to the one obtained previously by Ho [8].

If the vortex is nonsingular, however, the spinor $\zeta(\mathbf{r})$ will be identical everywhere on the boundary of the two-dimensional plane and it effectively represents a mapping from the surface of a three-dimensional sphere S^2 into the order-parameter space. We then need to consider the second homotopy group $\pi_2(G)$. For this we have that $\pi_2(\mathrm{SU}(2)) = \pi_2(\mathrm{SO}(3)) = 0$ and $\pi_2(\mathrm{U}(1) \times S^2) = Z$. Hence, nonsingular or coreless vortices are only possible for a spin-1 condensate with antiferromagnetic interactions. It therefore appears that the nonsingular spin texture discussed in Ref. [8], is topologically unstable and may be continuously deformed into the ground state by ''local surgery'' [21].

We are now in a position to discuss pointlike defects. Since the boundary of a three-dimensional gas is also the surface of a three-dimensional sphere, singular pointlike defects are also determined by the second homotopy group $\pi_2(G)$. Such topological excitations thus only exist in the case of a spin-1 Bose gas with antiferromagnetic interactions. We call these excitations 't Hooft and Polyakov monopoles [17], although it would be justifiable to call them singular skyrmions. For nonsingular pointlike defects, the spinor $\zeta(\mathbf{r})$ will again be identical on the boundary of the three-dimensional gas. As a result, the configuration space is compactified to the surface of a four-dimensional sphere S^3 and we need to determine the third homotopy group $\pi_3(G)$. For this we find $\pi_3(\mathrm{SU}(2)) = \pi_3(\mathrm{SO}(3)) = \pi_3(U(1) \times S^2) = Z$. Hence, nonsingular skyrmion excitations exist in all three cases.

B. skyrmion texture

We consider from now on only the case of a homogeneous and ferromagnetic spinor condensate. In the ground state, all spins are aligned along the direction of a uniform and sufficiently weak magnetic field, which we take to be along the z axis. The uniform magnetic field is needed only to direct the spins in the ground state, but it should not provide a substantial energy barrier for spin flips. The fact that we consider a homogeneous gas and not a confined one is only for simplicity and turns out not to be crucial for the practical applicability of our work. This is so because the, for our purposes, relevant length scale over which the skyrmion spin deformations take place is always of the order of the correlation length, which under typical experimental conditions is much less than the length scale for density gradients due to the confining potential. The skyrmion excitation is a space-dependent spin deformation of the ground state and can thus be represented by a position-dependent spinor $\zeta(\mathbf{r})$. A convenient way of introducing the position dependence in the spinor is to write it in terms of a position-dependent rotation that acts on the constant spinor ζ^{Z} associated with the ferromagnetic groundstate. In this manner, we have

$$\zeta(\mathbf{r}) = \exp\left\{ -\frac{i}{S}\mathbf{\Omega}(\mathbf{r}) \cdot \mathbf{S} \right\} \zeta^{\mathrm{Z}}. \tag{1}$$

Here, the constant spinor ζ^{Z} minimizes the Zeeman energy and is given by

$$\zeta^{Z}=\begin{cases}\begin{pmatrix}1\\0\end{pmatrix}, & S=\frac{1}{2}\\ \begin{pmatrix}1\\0\\0\end{pmatrix}, & S=1,\end{cases} \tag{2}$$

in the usual basis that diagonalizes S_z. Furthermore, $\mathbf{\Omega}(\mathbf{r})$ is a real vector function of $\mathbf{r}$. It parametrizes the ferromagnetic order-parameter space, which due to our incorporation of the factor $1/S$ in Eq. (1) is always a sphere of radius π. We point out that here and throughout the following, S can only take the values 1/2 or 1. The significance of Eq. (1) is that at a point $\mathbf{r}$ the spinor ζ^{Z} is rotated by an angle that equals $|\mathbf{\Omega}(\mathbf{r})|/S$ around the direction of $\mathbf{\Omega}(\mathbf{r})$. There is no restriction on the generality of spin textures produced by this means; it is merely a convenient parametrization of the order-parameter space in terms of $\mathbf{\Omega}(\mathbf{r})$. Since we are mostly interested in the equilibrium properties, we assume here for simplicity the maximally symmetric shape of the skyrmion, which is expected to have the smallest possible gradients. This means that we take

$$\mathbf{\Omega}(\mathbf{r})=\omega(r)\mathbf{r}/r\equiv\omega(r)\hat{\mathbf{r}}, \tag{3}$$

where the function $\omega(r)$ should obey the boundary conditions $\omega(0)=2\pi$ and $\lim_{r\to\infty}\omega(r)=0$ [22]. Thus, at these boundaries, the rotation operator in Eq. (1) becomes the identity and gives rise to $\zeta(\mathbf{r}=\mathbf{0})=\zeta(\mathbf{r}\to\infty)=\zeta^{Z}$. Furthermore, $\omega(r)$ should as a function of radius decrease monotonocally from 2π to 0, since this will correspond to the smallest gradient energy for the spin deformations. With this ansatz for $\mathbf{\Omega}(\mathbf{r})$ and its boundary conditions, we see that by traversing the whole configuration space, we exactly cover the order-parameter space twice, which is required to avoid a singular behavior of the spinor at $\mathbf{r}=\mathbf{0}$. Indeed, the boundary condition $\omega(0)=\pi$, which in first instance appears to be the right one as it leads to a spin texture that covers the order-parameter space only once, is physically unacceptable because it results in a singular behavior of the spinor $\zeta(\mathbf{r})$ and therefore in divergencies in the gradient energy. The reason for this singular behavior is that, given the maximally symmetric shape of the skyrmion, the spinor $\zeta(\mathbf{r})$ is always equal to ζ^{Z} in the origin. Note that apart from topological reasons, the condition $\lim_{r\to\infty}\omega(r)=0$ also ensures that the spin deformations associated with the skyrmion have a finite range, so that only a finite amount of energy is required to excite the skyrmion from the ground state. Thus, both on the z axis and far away from the center of the skyrmion, the spins are directed as in the ground state. From these general features, we can now draw a qualitative picture of the skyrmion texture. Suppose we approach the origin along a line through the origin, starting from a distance much larger than the range of the spin deformations. Then how does the average local spin behave as a function of distance? According to the above description of the rotation operator depicted in Fig. 1, the spin initially points up along the z axis, but by approaching the origin, it will start to rotate around the radial direction until we approach the origin and the spin points up again. It is essential that the spins complete an integer number of cycles equal to $1/S$ in order to have a nonzero topological winding number given by

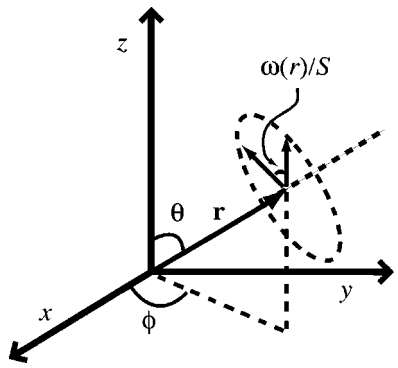

FIG. 1. Schematic figure representing the action of the spin rotation operator for a maximally symmetric skyrmion. At a position $\mathbf{r}$, the average spin vector is pointing initially in the z direction. The spin rotation operator rotates the spin vector around $\mathbf{r}$ by an angle $\omega(r)$.

$$N^{\mathrm{sk}}=\frac{3}{8\pi^4}\int d\mathbf{\Omega}=\frac{1}{16\pi^4}\int d\mathbf{r}\epsilon^{ijk}\epsilon_{\alpha\beta\gamma}\partial_i\Omega^{\alpha}\partial_j\Omega^{\beta}\partial_k\Omega^{\gamma}, \tag{4}$$

which in this case, is equal to one.

Summarizing, we have obtained the desired position dependence of $\zeta(\mathbf{r})$ in terms of a single function $\omega(r)$ that describes how the average local spin vector is tilted from its orientation in the ground state. This function and the local-density $n(\mathbf{r})$ represent the two degrees of freedom that describe the skyrmion and our next task is to determine their precise spacial dependence.

C. Energy functional

For a ferromagnetic spinor condensate, Ho [8] has shown that, within the mean-field approach, the energy functional in the absence of a magnetic field is given by

$$E[n,\zeta]\equiv\int d\mathbf{r}\left[\frac{\hbar^2}{2m}(\nabla\sqrt{n(\mathbf{r})})^2-\mu n(\mathbf{r})+\frac{\hbar^2}{2m}n(\mathbf{r})|\nabla\zeta(\mathbf{r})|^2+\frac{1}{2}T^{2B}n^2(\mathbf{r})\right], \tag{5}$$

where m is the mass of the atoms, μ is their chemical potential, and $T^{2B}=4\pi a\hbar^2/m$ is the appropriate coupling constant

that represents the strength of the interatomic interactions in terms of the positive scattering length a. The term $\hbar^2 n(\mathbf{r})|\nabla\zeta(\mathbf{r})|^2/2m$ represents the energy density associated with the gradients in the spin texture. It is this term that enforces the boundary-condition $\omega(0)=2\pi$, as discussed previously.

For sufficiently large distances, the gradient terms vanish and we infer from Eq. (5) that $\mu=n_\infty T^{2B}$, where $n_\infty=n(\mathbf{r}\to\infty)$. Using this, Eq. (5) may be put in a dimensionless form by scaling the lengths to the correlation length $\xi=1/\sqrt{8\pi a n_\infty}$, the density to n_∞, and the total energy to $\hbar^2 n_\infty \xi/2m$. In this manner, Eq. (5) becomes

$$\varepsilon[f,\zeta]\equiv\int d\boldsymbol{\rho}\left[(\nabla_{\boldsymbol{\rho}}\sqrt{f(\boldsymbol{\rho})})^2+f(\boldsymbol{\rho})|\nabla_{\boldsymbol{\rho}}\zeta(\boldsymbol{\rho})|^2+\frac{1}{2}f^2(\boldsymbol{\rho})-f(\boldsymbol{\rho})\right], \tag{6}$$

with $\boldsymbol{\rho}=\mathbf{r}/\xi$ and $n(\mathbf{r})=n_\infty f(\boldsymbol{\rho})$. The gradient term $|\nabla_{\boldsymbol{\rho}}\zeta(\boldsymbol{\rho})|^2$ is calculated in the Appendix explicitly as a function of $\omega(\rho)$. This is achieved by inserting in the usual basis the spin-1 and spin-1/2 matrices in the rotation operator, performing a power expansion and then using some properties of the powers of the spin matrices to sum the resulting infinite series into the following compact formula

$$|\nabla_{\boldsymbol{\rho}}\zeta(\boldsymbol{\rho})|^2=\begin{cases}2\left(\dfrac{\sin[\omega(\rho)]}{\rho}\right)^2+\left(\dfrac{d\omega(\rho)}{d\rho}\right)^2, & S=1/2\\ [5-\cos(2\theta)]\left(\dfrac{\sin[\omega(\rho)/2]}{\rho}\right)^2+\dfrac{1}{4}[3+\cos(2\theta)]\left(\dfrac{d\omega(\rho)}{d\rho}\right)^2, & S=1,\end{cases} \tag{7}$$

where θ is the azimuthal angle between $\boldsymbol{\rho}$ and the z axis.

Finally, the density profile $f(\boldsymbol{\rho})$ and the function $\omega(\rho)$ can be determined from the two coupled differential equations resulting from minimizing $\varepsilon[f,\zeta]$ with respect to $f(\boldsymbol{\rho})$ and $\omega(\rho)$, namely,

$$-\frac{\nabla_{\boldsymbol{\rho}}^2\sqrt{f(\boldsymbol{\rho})}}{\sqrt{f(\boldsymbol{\rho})}}+|\nabla_{\boldsymbol{\rho}}\zeta(\boldsymbol{\rho})|^2+f(\boldsymbol{\rho})-1=0, \tag{8}$$

and

$$\frac{1}{S}\langle f(\boldsymbol{\rho})\rangle_1\sin\left(\frac{\omega(\rho)}{S}\right)-2S\frac{d}{d\rho}\left[\rho^2\langle f(\boldsymbol{\rho})\rangle_2\left(\frac{d\omega(\rho)}{d\rho}\right)^2\right]=0, \tag{9}$$

where

$$\langle f(\boldsymbol{\rho})\rangle_1=\begin{cases}\dfrac{1}{4\pi}\displaystyle\int d\hat{\boldsymbol{\rho}}f(\boldsymbol{\rho}), & S=1/2\\ \dfrac{1}{4\pi}\displaystyle\int d\hat{\boldsymbol{\rho}}[5-\cos(2\theta)]f(\boldsymbol{\rho}), & S=1\end{cases} \tag{10}$$

and

$$\langle f(\boldsymbol{\rho})\rangle_2=\begin{cases}\dfrac{1}{4\pi}\displaystyle\int d\hat{\boldsymbol{\rho}}f(\boldsymbol{\rho}), & S=1/2\\ \dfrac{1}{4\pi}\displaystyle\int d\hat{\boldsymbol{\rho}}\dfrac{1}{4}[3+\cos(2\theta)]f(\boldsymbol{\rho}), & S=1.\end{cases} \tag{11}$$

In the spin-1 case, Eqs. (7) and (8) show that the density profile is, in principle, anisotropic. However, the anisotropy turns out to be rather small as we show explicitly in Sec. III.

D. Ansatz for $\omega(r)$

In principle, to calculate the exact skyrmion texture and density profile, we should now solve the two-coupled nonlinear differential equations that result from minimizing the energy functional with respect to $f(\boldsymbol{\rho})$ and $\zeta(\boldsymbol{\rho})$, namely, Eqs. (8) and (9). As an alternative, we employ here a rather simpler, though less rigorous, approach. We simplify the calculations by introducing an ansatz for $\omega(\rho)$ that takes explicitly into account the physical boundary conditions discussed in the previous section. Our ansatz is

$$\omega(\rho)=4\cot^{-1}(\rho/\lambda)^2, \tag{12}$$

where λ is a parameter that determines the radius at which $\omega(\rho)$ crosses over from 2π to 0 and physically corresponds to the size of the skyrmion. We see that this ansatz automatically satisfies the boundary-conditions $\omega(0)=2\pi$ and $\lim_{\rho\to\infty}\omega(\rho)=0$, as required. It should be noted here that the detailed functional behavior of $\omega(\rho)$ will turn out not to be crucial for our results on the skyrmion stability as long as it satisfies the prescribed boundary conditions and falls of monotonically. To substantiate this remark, we have performed also calculations using a number of different forms for $\omega(\rho)$ that satisfy the desired boundary conditions such as $\omega(\rho)=2\pi/[1+(\rho/\lambda)^2]$. We found, as expected, that the skyrmion energy only differs slightly from one function to the other and, in particular, that the energy is minimized for the function given in Eq. (12). Fortunately, this ansatz is also simpler to handle analytically.

III. STATIC AND DYNAMICAL STABILITY

The most important question about the skyrmion excitation is whether it is energetically stable or not. In other words, how does the energy of the skyrmion depends on its

size? As we show next, the answer to this question is that the skyrmion always tends to shrink to microscopic sizes to minimize its energy. Although this is an unfortunate result, it does not need to rule out an experimental observation of the skyrmion excitation as long as the typical time scale for this collapse is sufficiently long. Therefore, we also consider this problem after we have discussed the thermodynamical stability of the skyrmion.

For sufficiently large skyrmions, the gradients of the spinor $\zeta(\mathbf{r})$ are small and density fluctuations are therefore also small. The energy of the skyrmion may then be approximated by $(\hbar^2 n_\infty/2m)\int d\mathbf{r}|\nabla\zeta(\mathbf{r})|^2$. If the size of the skyrmion is of order of λ, this energy scales as λ. This indicates that the skyrmion tends to shrink in order to minimize its energy. However, for smaller sizes, the density fluctuations and their gradients start to grow and this simple argument no longer applies. For large skyrmions, Eq. (8) shows that the density fluctuations scale as $f(\rho)-1\approx|\nabla_{\boldsymbol{\rho}}\zeta(\boldsymbol{\rho})|^2\propto 1/\lambda^2$ and their energy contribution thus behaves as $1/\lambda$. Approaching smaller values of λ, the kinetic-energy term in Eq. (8) increases and the density fluctuations will scale with a power of λ that is greater than -2, because otherwise, the density would become negative at some point. As a result, the energy will scale with a power of λ that is different from one. Therefore, there is, in principle, a chance for stability if the energy associated with the density fluctuations is at some point increasing when λ becomes smaller. To investigate this possibility, we need to calculate the energy as a function of λ exactly for all values of λ. If the energy function possesses a (local) global minimum for a finite λ, then the skyrmion is energetically (meta)stable. We have indeed calculated this energy curve, the details can be found in Sec. III B below, and it turns out that the skyrmion energy actually increases monotonically with λ. This means that a skyrmion of any finite size is energetically unstable and will tend to decrease to zero size. Of course, this condition holds within the Gross-Pitaevskii theory, which describes only the long-wavelength physics. Corrections to this theory will lead to a finite, but microscopically small size of the skyrmion. However, as mentioned previously, for observing the skyrmion experimentally, it is important to know the time scale for its collapse since it could be larger than the lifetime of the condensate itself due to various inelastic processes, such as two- and three-body collisions and, in an optical trap, photon absorption.

From our analysis of the skyrmion shrinking rate, it turns out that there are two size regimes with different shrinking mechanisms. The first is for skyrmions with a size λ that is much larger than the correlation length of the gas. The second regime is for much smaller skyrmions with sizes of the order of the correlation length or less. In the next two sections we calculate the skyrmion energy and estimate its shrinking rate in these two regimes.

A. Large skyrmions

As mentioned earlier, large skyrmions have a size λ that satisfies $\lambda\gg\xi=1/\sqrt{8\pi a n_\infty}$, where ξ is the correlation length of a homogeneous gas of average density n_∞ and s-wave interatomic scattering length a. In this section, we express the lagrangian of the skyrmion in terms of a time-dependent skyrmion size $\lambda(t)$. An equation of motion for $\lambda(t)$ is then derived. It should be noted here that comparison between our calculation in this section and experiment is only meaningful for skyrmion sizes much less than the condensate size since this calculation is for a homogeneous system and does not take into account the effect of the trap. The two conditions thus imply that the spinor condensate is deep in the Thomas-Fermi regime.

For large skyrmions, the gradients in the spinor $\zeta(\mathbf{r})$ are small and therefore the fluctuations in the density $\delta n(\mathbf{r})=n(\mathbf{r})-n_\infty$ are also small compared to the average density n_∞. The energy of the skyrmion can thus be determined by an harmonic approximation to the Gross-Pitaevskii energy functional given in Eq. (5). To second order in $\delta n(\mathbf{r})$ it is given by

$$E[n,\zeta]=\frac{1}{2}\int d\mathbf{r}\int d\mathbf{r}'\ \delta n(\mathbf{r})\chi^{-1}(\mathbf{r}-\mathbf{r}')\delta n(\mathbf{r}') + \int d\mathbf{r}\, n(\mathbf{r})\left(\frac{\hbar^2}{2m}|\nabla\zeta(\mathbf{r})|^2-\gamma\mathbf{B}\cdot\langle\mathbf{S}\rangle(\mathbf{r})\right), \tag{13}$$

where $\chi(\mathbf{r}-\mathbf{r}')$ is the static density-density response function, which is defined by

$$\frac{\hbar^2}{4mn_\infty}(-\nabla^2+16\pi a n_\infty)\chi(\mathbf{r}-\mathbf{r}')=\delta(\mathbf{r}-\mathbf{r}') \tag{14}$$

but explicitly reads

$$\chi(\mathbf{r}-\mathbf{r}')=\frac{mn_\infty}{\pi\xi\hbar^2}\frac{\exp(-\sqrt{2}|\mathbf{r}-\mathbf{r}'|/\xi)}{|\mathbf{r}-\mathbf{r}'|/\xi}. \tag{15}$$

B is either a fictitious, caused by resonant rf fields, or a real homogeneous magnetic field, and γ is the corresponding magnetic moment of the atoms in the trap. Considering first the ideal case of zero magnetic-field **B** and solving for the density fluctuations induced by the spin texture, the lagrangian takes the form $L[\zeta]=T[\zeta]-E[\zeta]$, where

$$E[\zeta]=\int d\mathbf{r}n_\infty\frac{\hbar^2}{2m}|\nabla\zeta(\mathbf{r},t)|^2 - \frac{\hbar^4}{8m^2}\int d\mathbf{r}\int d\mathbf{r}'|\nabla\zeta(\mathbf{r},t)|^2\chi(\mathbf{r}-\mathbf{r}')|\nabla\zeta(\mathbf{r}',t)|^2, \tag{16}$$

and

$$T[\zeta]=\int d\mathbf{r} n_\infty \zeta^\dagger(\mathbf{r},t) i\hbar \frac{\partial}{\partial t}\zeta(\mathbf{r},t) + \frac{1}{2}\int d\mathbf{r}\int d\mathbf{r}'\, \zeta^\dagger(\mathbf{r},t) i\hbar \frac{\partial}{\partial t}\zeta(\mathbf{r},t) \times \chi(\mathbf{r}-\mathbf{r}')\zeta^\dagger(\mathbf{r}',t) i\hbar \frac{\partial}{\partial t}\zeta(\mathbf{r}',t), \tag{17}$$

as a result of the fact that in Gross-Pitaevskii theory, the action for the ferromagnetic condensate contains the time-derivative term $\int dt \int d\mathbf{r} n(\mathbf{r},t)\zeta^\dagger(\mathbf{r},t) i\hbar \partial\zeta(\mathbf{r},t)/\partial t$. The equation of motion for $\lambda(t)$ may be derived from the above lagrangian by substituting our ansatz for $\zeta(\mathbf{r},t)$ given in Eqs. (1), (3), and (12). In the present limit, $\lambda \gg \xi$ and the second term in the energy $E[\zeta]$ is much smaller than the first one. Therefore, we do not take it into account. Using the explicit expressions for $|\nabla\zeta(\mathbf{r})|^2$ from Eq. (7), the energy is calculated to be

$$E[\lambda]=C\frac{\hbar^2}{2m}n_\infty\lambda, \tag{18}$$

where $C=(29-20S)\sqrt{2}\pi^2$. For the time-dependent contribution $T[\zeta]$, we calculate first $\zeta^\dagger(\mathbf{r},t)\partial\zeta(\mathbf{r},t)/\partial t$, which turns out to be equal to $-i\dot{\lambda}(\partial\omega/\partial\lambda)\cos\theta$ for both $S=1/2$ and $S=1$, where the dot denotes a derivative with respect to time. Since $\partial\omega/\partial\lambda$ is an even function in r, the first term of $T[\zeta]$ vanishes. Thus, $T[\lambda]$ turns out to be

$$T[\lambda]=\frac{\lambda}{\sqrt{2}a}m\dot{\lambda}^2. \tag{19}$$

So, combining Eqs. (18) and (19), we see that the action for the dynamical variable $\lambda(t)$ is equivalent to that of a particle with a position-dependent effective mass $m^*=\sqrt{2}m\lambda/a$ in the linear potential $V(\lambda)=C\hbar^2 n_\infty\lambda/2m$. Scaling again λ to the correlation length ξ, the number $\sqrt{2}\lambda/a$ takes the form $\lambda/\sqrt{4\pi n_\infty a^3}$. Experimentally, the dimensionless parameter $n_\infty a^3$ is typically of order 10^{-5}. This leads to an effective mass $m^*\approx 10^2\lambda m$. Thus, a typical adult skyrmion mass, for say $\lambda=10$, is 10^3 times atomic mass. Finally, the equation of motion for $\lambda(t)$ reads

$$2\lambda\ddot{\lambda}+\dot{\lambda}^2+c=0, \tag{20}$$

where $c=(29-20S)\pi$. In this equation, lengths are again scaled to the correlation length ξ and time is scaled to the correlation time $\tau=2m\xi^2/\hbar$. In these units the condition of validity of this equation is $\lambda\gg 1$. For the initial conditions $\lambda(0)=\lambda_0$ and $\dot{\lambda}(0)=0$, we find that

$$\lambda=\lambda_0\left(1-\frac{c}{4\lambda_0^2}t^2\right) \tag{21}$$

is a solution to Eq. (20). This formula shows that large skyrmions decrease with a rate $\gamma_{\text{large}}\approx\sqrt{c}/2\lambda_0\tau$, which indicates that spin-1/2 skyrmions decrease almost twice as fast as spin-1 skyrmions. In both cases, one can make the shrinking rate smaller by exciting larger skyrmions. For realistic estimates of these shrinking rates, we restore the units in the above expression for γ_{large}. For ^{87}Rb spin-1/2 condensate of central density 10^{-11} cm^{-3}, the rate then reads $\gamma_{\text{large}}\approx 18.06\xi/\lambda$ sec^{-1}.

B. Small skyrmions

The cruicial difference between large skyrmions and small skyrmions, apart from the size difference, is that density fluctuations for small skyrmions are much more important than for the large skyrmions. The density depletion produced by the spin gradients increases for smaller skyrmions, and thus, we cannot consider the density to be essentially uniform anymore. Therefore, the linear-response approach followed in the previous section does not apply. To take the density fluctuations properly into account, we need to use the full energy functional. As already mentioned, it leads to a size dependence of the skyrmion energy, such that the skyrmion tends to decrease to zero size. The shrinking process, however, is now fundamentally different and more complicated than that for the large skyrmions. In this case, while the skyrmion is shrinking, the density becomes increasingly depleted in a region that forms a closed shell around the center of the skyrmion. For sufficiently small λ, the depletion will be so large that the atoms inside the closed shell are essentially isolated from the atoms outside the shell. This will considerably slow down the collapse of the skyrmion since the atoms within the shell need to tunnel over a potential barrier to escape to the other side of the shell and to enable the skyrmion to decrease further. It turns out that the size of the skyrmion at this stage is of the order of the correlation length and the lifetime of the skyrmion due to the above tunneling process can be much larger than the lifetime of the condensate itself.

1. Density profile and texture

With our ansatz for $\omega(\rho)$ in Eq. (12) the problem is significantly simplified since to determine the density profile we only have to solve Eq. (8), which is basically a nonlinear Schrödinger equation with some external potential $|\nabla_{\boldsymbol{\rho}}\zeta(\boldsymbol{\rho})|^2$. Substituting our ansatz for $\omega(\rho)$ in Eq. (7), the latter takes the form

$$|\nabla_{\boldsymbol{\rho}}\zeta(\boldsymbol{\rho})|^2 = \begin{cases} 32\left(\dfrac{\rho}{\lambda^2}\right)^2\dfrac{[3+2(\rho/\lambda)^4+3(\rho/\lambda)^8]}{[1+(\rho/\lambda)^4]^4}, & S=1/2 \\ 4(17+3\cos\theta^2)\left(\dfrac{\rho}{\lambda^2}\right)^2\dfrac{1}{[1+(\rho/\lambda)^4]^2}, & S=1. \end{cases} \tag{22}$$

This is an off-centered potential barrier with a maximum height of $24.3/\lambda^2$ at $r\approx 0.68\lambda$, for $S=1/2$ and a maximum height equal to $3\sqrt{3}(17+3\cos^2\theta)/4\lambda^2$ at $r=\lambda/3^{1/4}$ for $S=1$. Using this form for $|\nabla\zeta(\boldsymbol{\rho})|^2$, we solve Eq. (8) numerically for one particular value of λ. Then we use the resulting

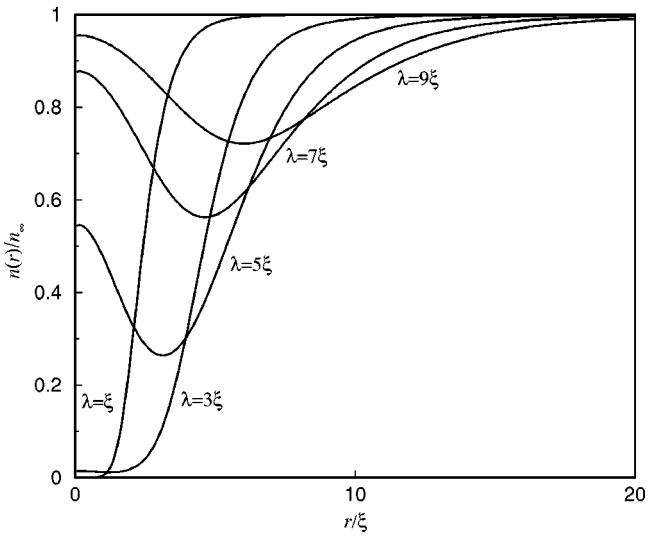

FIG. 2. The density profile for a skyrmion in a spin-1/2 condensate for different values of λ. These curves are the numerical solutions of Eq. (8) using Eq. (22).

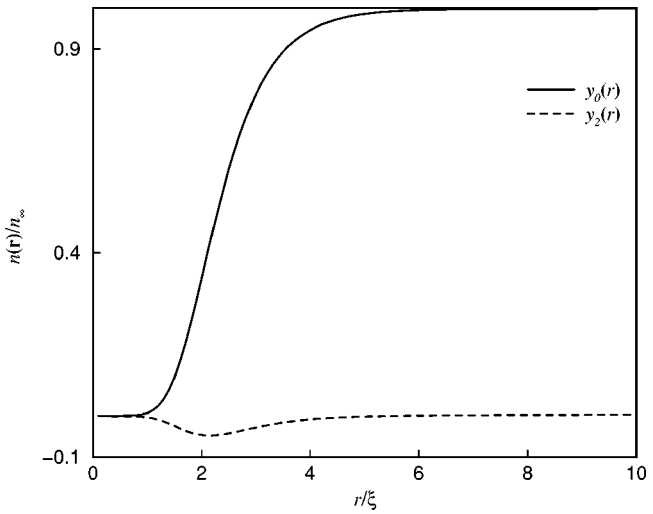

FIG. 3. Density profile for a skyrmion in a spin-1 spinor condensate with a size of $\lambda=\xi$. The solid curve represents the isotropic part of $n(\mathbf{r})$ and the dashed curve represents the anisotropic part. These are the numerical solution of Eqs. (24) and (25).

density distribution $f(\boldsymbol{\rho})$ to calculate the energy for that particular value of λ. Performing the same calculation for different values of λ, we finally obtain the energy of the skyrmion as a function of λ, from which we can judge the stability of the skyrmion.

For the spin-1/2 case, the density profile for various values of λ is shown in Fig. 2. In the case of $S=1$, the calculation is more complicated due to the angular dependence of $|\boldsymbol{\nabla}_{\boldsymbol{\rho}}\zeta(\boldsymbol{\rho})|^2$. This complication is handled by noticing that $|\boldsymbol{\nabla}_{\boldsymbol{\rho}}\zeta(\boldsymbol{\rho})|^2$ can be rewritten in terms of $Y_{00}(\theta,\phi)$ and $Y_{20}(\theta,\phi)$ only, where $Y_{lm}(\theta,\phi)$ are the usual spherical harmonics. We thus also expand Eq. (8) in the spherical harmonics up to $l=2$ using

$$\sqrt{f(\boldsymbol{\rho})}=y_0(\rho)Y_{00}(\theta,\phi)+y_2(\rho)Y_{20}(\theta,\phi). \tag{23}$$

Then, two coupled equations can be obtained by taking the $l=0$ and $l=2$ components of Eq. (8). Specifically, we substitute Eq. (23) into Eq. (8) and multiply by $Y_{00}(\theta,\phi)$ and $Y_{20}(\theta,\phi)$, respectively, and then perform an angular integration. The resulting equations take the form

$$-\nabla_\rho^2 y_0+\frac{16}{\lambda^2}\frac{(\rho/\lambda)^2}{[1+(\rho/\lambda)^4]^2}\left(4y_0+\frac{1}{\sqrt{5}}y_2\right)+\frac{1}{4\pi}y_0^3 +\frac{3}{4\pi}y_0y_2^2+\sqrt{\frac{5}{14\pi}}y_2^3=y_0 \tag{24}$$

and

$$-\nabla_\rho^2 y_2+\frac{6}{\rho^2}y_2+\frac{16}{\lambda^2}\frac{(\rho/\lambda)^2}{[1+(\rho/\lambda)^4]^2}\left(\frac{1}{\sqrt{5}}y_0+\frac{58}{7}y_2\right) +\frac{3}{4\pi}y_2y_0^2+3\sqrt{\frac{5}{14\pi}}y_0y_2^2+\frac{15}{28\pi}y_2^3=y_2, \tag{25}$$

where $\nabla_\rho^2=(1/\rho^2)\partial/\partial\rho[\rho^2(\partial/\partial\rho)]$. The result of the numerical solutions of these two equations is presented in Fig. 3. From this figure, it is clear that the anisotropic part of $f(\boldsymbol{\rho})$, which is represented by $y_2(\rho)$, is considerably smaller than the isotropic part. This result will be employed in the following to simplify the energy calculation by neglecting the angular dependence of $f(\boldsymbol{\rho})$. Note that for $S=1/2$, this is not an approximation.

Having specified $\omega(r)$ enables also a detailed visualization of the skyrmion texture by calculating the average spin projections, i.e., $\langle S_x\rangle=\zeta^\dagger(\mathbf{r})S_x\zeta(\mathbf{r})$, $\langle S_y\rangle$, and $\langle S_z\rangle$. In Fig. 4, we plot these quantities as a function of r for the spin-1 case using, again, $\lambda=\xi$. Similar plots for the spin-1/2 case can be found in our previous work [16]. The skyrmion can be best visualized from its $\langle S_z\rangle(\mathbf{r})$ component, which is shown in the Appendix to be equal to

$$\langle S_z\rangle=\cos^2\theta+\cos\omega\sin^2\theta. \tag{26}$$

This expression is used to produce the two upper false-color figures in Fig. 4. These figures show clearly that the skyrmion corresponds to a torodial region. Along the inner radius of the torus, the direction of the average spin vectors is opposite to that in the ground state. An interesting property shows up when we calculate the associated superfluid velocity $\mathbf{v}_s(\mathbf{r})=-i\hbar\zeta^\dagger(\mathbf{r})\boldsymbol{\nabla}\zeta(\mathbf{r})/m$. This is given by

$$\mathbf{v}_s=\hbar\left[\hat{\mathbf{r}}\cos\theta\frac{d\omega}{dr}-\hat{\boldsymbol{\theta}}\frac{1}{r}\sin\theta\sin\omega-\hat{\boldsymbol{\phi}}\frac{2}{r}\sin\theta\sin^2(\omega/2)\right]. \tag{27}$$

From the above two expressions we find that the superfluid velocity is such that the atoms are simultaneously rotating around the inner radius of the torus and around the z axis. This corresponds to a spiraling motion around the inner radius of the torus. The speed is maximum in the center of the torus. Furthermore, the maximum depletion of the density

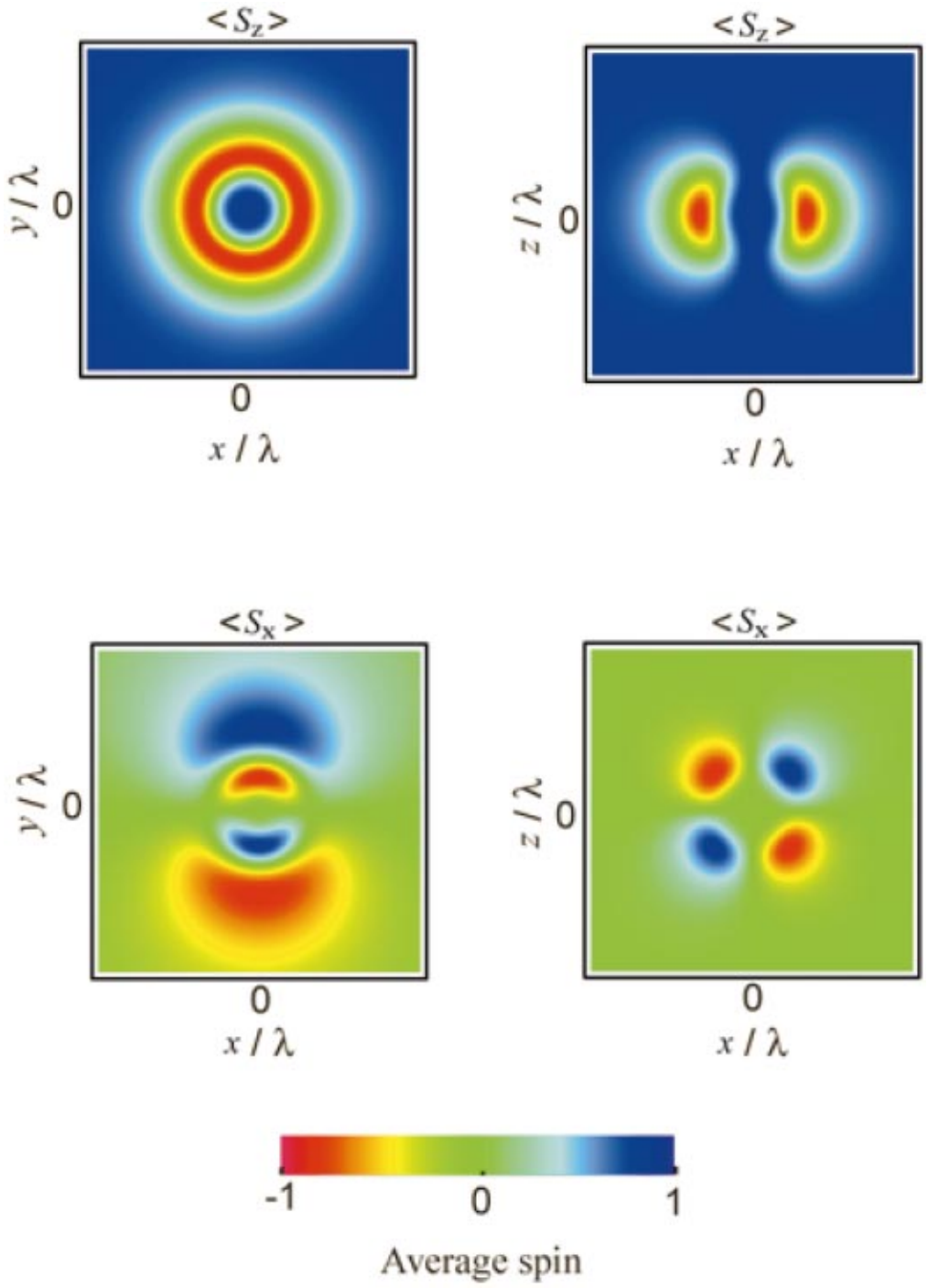

FIG. 4. (Color) False-color figures representing the average spin $\langle \mathbf{S} \rangle(\mathbf{r})$ for a skyrmion in a spin-1 condensate in different Cartesian planes. The size of the skyrmion is taken here to be equal to $\lambda = \xi$. The $\langle S_y \rangle$ figures can be obtained from the $\langle S_x \rangle$ figures by using the axial symmetry of the texture.

takes place at the maximum of $|\nabla \zeta(\mathbf{r})|^2$, which turns out to be in the center of the torus, where the spin vector is also completely flipped, i.e., $\langle S_z \rangle = -1$. In the case of a spin-1/2 condensate, the spin texture consists of two torii. The velocity field in this case is such that atoms spiral around the center of one torus clockwise and along the center of the other torus counterclockwise, but for both torii, the atoms rotate around the z axis in the same direction. The spins are completely flipped along the inner radii of the two torii. The density is mostly depleted along a radius that is slightly smaller than the inner radius of the larger torus. The shift is only approximately three percent of the size of the skyrmion.

2. Equilibrium state

The outcome of the calculation in the previous subsection is the skyrmion density profile as a function of λ. Therefore,

the energy of the skyrmion, determined from Eq. (5), is now also a function of λ. The skyrmion will be energetically stable if this energy $E[\lambda]$ has a local or global minimum and the equilibrium size of the skyrmion will be equal to the value of λ at that minimum. It should be noted that what we call the energy of the skyrmion is actually the grand-canonical energy. This implies that the density profile is solved by using a fixed chemical potential for all values of λ. Consequently, the number of atoms associated with the skyrmion excitation, which equals $|\int d\mathbf{r}[n(\mathbf{r})-n_\infty]|$, is also λ dependent. (The subtracted term is to cancel the divergent part coming from the fact that the system is infinite. In a confined system, there is no need to make this subtraction.) It may therefore not be immediately clear that minimizing the grand-canonical energy is appropriate. In principle, we must minimize the true energy of the skyrmion at a fixed number of atoms. We now explicitly show though, that these procedures are equivalent.

Let us take the number of atoms in the system equal to N. This means that in the absence of the skyrmion $\int d\mathbf{r} n_\infty = N$. Suppose we now put in a skyrmion of size λ in the condensate without affecting the asymptotic density, i.e., $n(\mathbf{r}\to\infty) = n_\infty$. Due to the depletion of the density near the center of the skyrmion, the total number of atoms associated with this density profile is slightly less than N by an amount $\Delta N(\lambda) = \int d\mathbf{r}[n_\infty - n(\mathbf{r},\lambda)]$. Physically, this means that to produce this skyrmion we have to remove $\Delta N(\lambda) \ll N$ atoms to the edge of the spinor condensate. If we, however, want to produce a skyrmion with the same number of atoms in the condensate, we have to adjust the asymptotic density. This implies that a reasonable approximation to the density profile is actually $[N/(N-\Delta N)]n(\mathbf{r},\lambda)$ because then

$$\frac{N}{N-\Delta N}\int d\mathbf{r} n(\mathbf{r},\lambda) = N\frac{N-\Delta N(\lambda)}{N-\Delta N(\lambda)} = N. \tag{28}$$

Using this density profile to calculate the true energy of the skyrmion and expanding the various terms in it up to first order in $\Delta N(\lambda)/N$, we reproduce exactly the grand-canonical energy $E[\lambda]$. Thus, we conclude that minimizing the canonical energy with a fixed number of atoms is indeed equivalent to minimizing the grand-canonical energy at a fixed chemical potential, and thus, with a changing number of atoms. The second method is clearly more convenient numerically since it is difficult to keep the number of atoms fixed for each value of λ.

In Fig. 5, we show our final result of this calculation, where we have taken $n(\mathbf{r})$ to be isotropic, since in the previous section we saw that the angular dependence of $n(\mathbf{r})$ can indeed be neglected. In detail, we have plotted here $E[n(r)]-\mu n(r)-(E[n_\infty]-\mu n_\infty)$ against λ. Again, we subtract the divergent part due to the infiniteness of the system. Unfortunately, both of the two curves do not have a minimum for any finite λ and only contain a global minimum at $\lambda = 0$. This means that, according to this figure, the skyrmion is energetically unstable, i.e., if the skyrmion is created with a finite size it will ultimately decrease to zero size. This process is clearly seen in Fig. 2, where we plot the skyrmion density profile for different values of λ. In the next section,

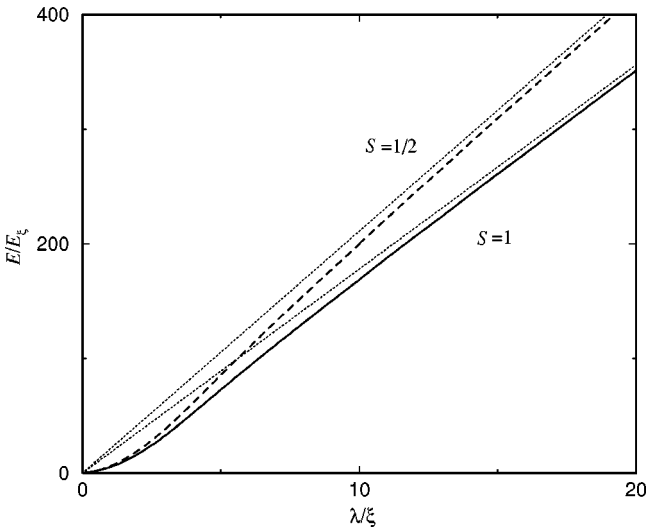

FIG. 5. Energy of a skyrmion as a function of its size. Plotted with the solid (dashed) curve is the energy for a spin-1 (spin-1/2) spinor condensate. The dotted asymptotes are the large λ limit of the energy, which is linear in λ and is given by the spin gradient term in the energy functional only. Energy is in units of the correlation energy $E_\xi = (4\pi\hbar^2/2m\xi^2)$.

we examine this shrinking process for the small skyrmions more closely. In particular, we again look at the time scale over which this shrinking occurs and find that for current experimental situations it is of the order of, or even longer than, the lifetime of the condensate itself.

Finally, we mention here some remarks about the effect of a homogeneous external magnetic field and the slight differences in the scattering lengths of the different hyperfine spin states. In the presence of a homogeneous magnetic-field **B**, it will be energetically unfavorable to flip spins. Therefore, this will lead to a further reduction in the spin of the skyrmion and, thus, not to a stabilization. A slight difference in the various scattering lengths Δa, as appropriate for the spin-1/2 ^{87}Rb condensate [23], leads to an additional term in the energy expression for the spinor condensate of the form $(4\pi\Delta a\hbar^2/m)\int d\mathbf{r} n(\mathbf{r})\langle S_z\rangle(\mathbf{r})$, which has exactly the same effect as an external magnetic field. It cannot stabilize the skyrmion either.

3. Shrinking rate

The goal of this section is to estimate the time scale over which the skyrmion decreases to zero size. A key element in understanding the dynamics of this process is the behavior of the potential barrier produced by the spin gradients $|\nabla\zeta(\mathbf{r})|^2$ when λ goes to zero. This potential is written down explicitly in Eq. (22). When λ is decreasing, the location of the off-centered peak of this potential is approaching the origin as λ and its height is increasing as $1/\lambda^2$. This potential is thus an isotropic three-dimensional repulsive shell that is increasing in strength as it becomes smaller. We denote from now on the atoms inside this shell by the ''core'' atoms and the ones outside by the ''external'' atoms. We have seen in the previous section that, in principle, the skyrmion is unstable and that it is energetically favorable for the skyrmion

to decrease to zero size irrespective of the initial size. Let us therefore consider a skyrmion of a large initial size, such that the height of the corresponding potential barrier is less than the chemical potential $\mu = n_\infty T^{2B}$ of the system. The density distribution will be almost uniform everywhere except in the region where the barrier has its maximum height. In this region, the density profile will be depleted only slightly. When the skyrmion starts to decrease, the depletion of the density becomes larger, since the height of the barrier increases. This is achieved physically by transporting the core atoms over the potential barrier to the external region. So the central density $n(\mathbf{0})$ decreases while the skyrmion is shrinking, as can be seen in Fig. 2. At a certain size, the height of the barrier becomes equal to the chemical potential of the atoms at large distances. As the skyrmion decreases even further, the barrier height actually exceeds the chemical potential. At this stage, the shrinking process slows down significantly since the core atoms will now have to tunnel through a potential barrier. The rate of this process will be characterized by the usual WKB tunneling rate, which we calculate now.

To calculate this tunneling rate, we assume that the skyrmion has decreased to a size for which the barrier is so high that the overlap between the wave functions of the core atoms and the external atoms is exponentially small. The tunneling rate will then be determined by the chemical potential of the core atoms, as well as the barrier height. We consider the situation that there are $N_{\rm core}$ core atoms with a chemical potential $\mu_{\rm core}$ less than the height of the barrier. Note that physically we must always have that $\mu_{\rm core} \geqslant \mu$, since the collapse of the skyrmion will squeeze the atoms inside the core. For small r/λ, we notice from Eq. (22) that the potential $(\hbar^2/2m)|\boldsymbol{\nabla}\zeta(\mathbf{r})|^2$ may be approximated by a harmonic potential well with a characteristic frequency ω_0 that equals $\sqrt{48}\hbar/m\lambda^2$ for $S=1/2$ and $\sqrt{32}\hbar/m\lambda^2$ for $S=1$. It thus has a characteristic length $l=\lambda/\sqrt{96}$ for $S=1/2$ and $l=\lambda/8$ for $S=1$. This allows us to use a Thomas-Fermi approximation, the validity of which will be discussed below, to calculate $\mu_{\rm core}$. Moreover, the tunneling rate is calculated using the following WKB expression [24]

$$\gamma_{small} \approx \frac{\omega_0}{2\pi}\exp\left[-2\int_{r_1}^{r_2} dr\,\sqrt{|\boldsymbol{\nabla}\zeta|^2 - 2m\mu_{\rm core}/\hbar^2}\right]. \tag{29}$$

The radial points r_1 and r_2 are the points where $(\hbar^2/2m)|\boldsymbol{\nabla}\zeta(\mathbf{r})|^2$ and $\mu_{\rm core}$ intersect. The use of a Thomas-Fermi approximation is justified when the mean-field interaction energy of the core atoms is larger than the spacing between the lowest energy levels of the harmonic potential well. Specifically, the ratio $2Na/l = 2\sqrt{96}Na/\lambda$ should be bigger than one. Figure 6(a) shows the equilibrium size of the small skyrmion, which is calculated by minimizing the total energy while keeping the number of the core atoms constant, as a function of the number of the core atoms $N_{\rm core}$. From this figure, we observe that the above ratio equals approximately 1 for $N_{\rm core}=4$ and it increases for larger $N_{\rm core}$. For experimental situations, Fig. 6(b) shows that the skyrmion can live for a time ranging from seconds to hundreds of seconds, which is long enough to be observed. It should be noted that the above expression, which is based on a variational approach, somewhat overestimates the lifetime of the skyrmion. However, this is not crucial for our purposes, since by shrinking slightly, the lifetime of the skyrmion increases considerably.

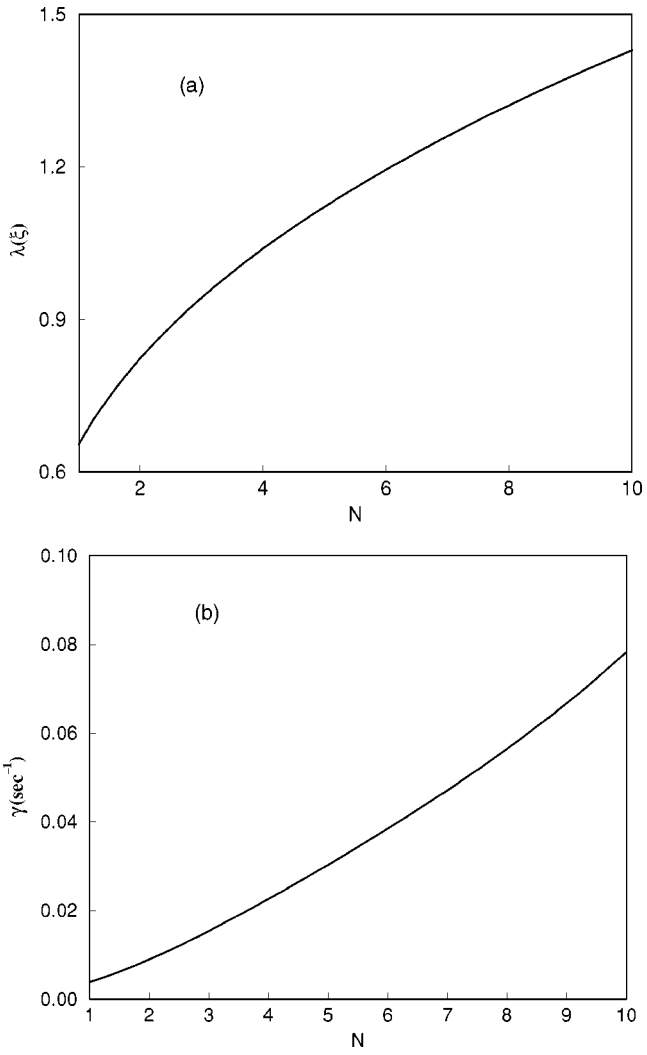

FIG. 6. Shown are (a) the small skyrmions size as a function of the number of core atoms and (b) the shrinking rate of skyrmion as a function of the number of core atoms. This calculation was performed for a ^{87}Rb spin-1/2 condensate with a scattering length of $a=5.4$ nm.

IV. SKYRMION DYNAMICS

A very important dynamical variable of the skyrmion arises from the fact that the Euler-Lagrange equations for the skyrmion spin texture is invariant under a space-independent rotation of the average local spin $\langle\mathbf{S}\rangle(\mathbf{r})$ around the magnetic-field direction $\hat{\mathbf{B}}$ [25]. Mathematically, this means that if the spinor $\zeta^{\rm sk}(\mathbf{r})$ describes a skyrmion, then $\exp\{-i\vartheta\hat{\mathbf{B}}\cdot\mathbf{S}\}\zeta^{\rm sk}(\mathbf{r})$ describes also a skyrmion with the same winding number and energy. The dynamics of the variable $\vartheta(t)$ associated with this symmetry is determined by the full action for the spin texture $S[\zeta]=\int dt(T[\zeta]-E[\zeta])$, where

$E[\zeta]$ and $T[\zeta]$ are given by Eqs. (16) and (17) with n_∞ replaced by the density profile $n(\mathbf{r})$ of the skyrmion and $\chi(\mathbf{r}-\mathbf{r}')$ should now be interpreted as the exact density-density correlation function in the presence of the skyrmion. Hence, substituting $\zeta(\mathbf{r},t)=\exp\{-i\vartheta(t)\hat{\mathbf{B}}\cdot\mathbf{S}\}\zeta^{\mathrm{sk}}(\mathbf{r})$ and making use of the conservation of total particle number N to introduce the change of the average local spin projection on the magnetic field $\langle\Delta S_{||}\rangle(\mathbf{r})=\hat{\mathbf{B}}\cdot\langle\mathbf{S}\rangle(\mathbf{r})-NS$ induced by the skyrmion, we obtain, apart from an unimportant boundary term, that the dynamics of the rotation angle $\vartheta(t)$ is determined by the action

$$S[\vartheta]=\int dt\left\{\frac{\partial\vartheta(t)}{\partial t}\hbar\langle\Delta S_{||}^{\mathrm{tot}}\rangle+\frac{1}{2}I\left(\frac{\partial\vartheta(t)}{\partial t}\right)^2\right\}, \quad (30)$$

where $\langle\Delta S_{||}^{\mathrm{tot}}\rangle$ is the change of the total spin along the magnetic-field direction and the ''moment of inertia'' of the skyrmion equals

$$I=\hbar^2\int d\mathbf{r}\int d\mathbf{r}'\langle\Delta S_{||}\rangle(\mathbf{r})\chi(\mathbf{r},\mathbf{r}')\langle\Delta S_{||}\rangle(\mathbf{r}'). \quad (31)$$

For a large skyrmion, this integral can be performed by substituting $\langle\Delta S_{||}\rangle=\langle S_z\rangle-NS$ and using Eq. (14) for $\chi(\mathbf{r},\mathbf{r}')$. The explicit expressions for $\langle S_z\rangle$ can be found in the Appendix. An even simpler expression for $\chi(\mathbf{r},\mathbf{r}')$ may be obtained by neglecting the gradient terms in Eq. (14). Then

$$\chi(\mathbf{r},\mathbf{r}')=\frac{m}{4\pi\hbar^2 a}\delta(\mathbf{r}-\mathbf{r}'). \quad (32)$$

Using this approximation we find

$$I=\begin{cases}\dfrac{53\pi}{40\sqrt{2}}\dfrac{\lambda^3}{a}m, & S=1/2\\[2ex] \dfrac{14\pi}{15\sqrt{2}}\dfrac{\lambda^3}{a}m, & S=1.\end{cases} \quad (33)$$

The importance of this result is twofold. First, from the action in Eq. (30), we see that at the quantum level, the Hamiltonian for the dynamics of the wave function $\Psi(\vartheta,t)$ becomes

$$H=\frac{1}{2I}\left(\frac{\hbar}{i}\frac{\partial}{\partial\vartheta}-\hbar\langle\Delta S_{||}^{\mathrm{tot}}\rangle\right)^2. \quad (34)$$

Therefore, the ground-state wave function is given by $\Psi_0(\vartheta)=e^{iK\vartheta}/\sqrt{2\pi}$, with K an integer that is as close as possible to $\langle\Delta S_{||}^{\mathrm{tot}}\rangle$. In this way, we thus recover the fact that according to quantum mechanics, the total number of spin flips associated with the skyrmion texture must be an integer. More precisely, we have actually shown that the many-body wave function describing the skyrmion is an eigenstate of the operator $\hat{\mathbf{B}}\cdot\mathbf{S}^{\mathrm{tot}}$ with eigenvalue $NS-K$. Note that physically this is equivalent to the way in which ''diffusion'' of the overall phase of a Bose-Einstein condensate leads to the conservation of particle number [26,27].

Furthermore, the existence of this internal degree of freedom becomes especially important when we deal with more than one skyrmion in the condensate. In that case, every skyrmion may have its own orientation and we expect the interaction between two skyrmions to have a Josephson-like contribution proportional to $\cos(\vartheta_1-\vartheta_2)$. As a result, the phase diagram of a gas of skyrmions may become extremely rich and contain both quantum as well as classical, i.e., nonzero temperature, phase transitions [25]. In this context, it is interesting to mention two important differences with the situation in the quantum Hall effect. First, the fact that the spin projection K of the skyrmion is an integer shows that these excitations have an integer spin and are therefore bosons [28]. In the quantum Hall case, the skyrmions are fermions with half-integer spin, due to the presence of a topological term in the action $S[\zeta]$ for the spin texture [29]. Second, in a spinor Bose-Einstein condensate, the skyrmions are not pinned by disorder and are, in principle, free to move. Both differences will clearly have important consequences for the many-body physics of a skyrmion gas.

Focusing again on the single skyrmion dynamics, we can make the last remark more quantitative by using the ansatz $\zeta(\mathbf{r},t)=\zeta^{\mathrm{sk}}[\mathbf{r}-\mathbf{u}(t)]$ for the texture of a moving skyrmion, which is expected to be accurate for small velocities $\partial\mathbf{u}(t)/\partial t$. Considering for illustrative purposes again, only the isotropic approximation, we find in a similar way as before that the action for the center-of-mass motion of the skyrmion becomes

$$S[\mathbf{u}]=\int dt\,\frac{1}{2}M\left(\frac{\partial\mathbf{u}(t)}{\partial t}\right)^2, \quad (35)$$

where the mass is now simply given by

$$M=\frac{m^2}{3}\int d\mathbf{r}\int d\mathbf{r}'\chi(\mathbf{r},\mathbf{r}')\langle\mathbf{v}_s\rangle(\mathbf{r})\cdot\langle\mathbf{v}_s\rangle(\mathbf{r}') \quad (36)$$

in terms of the superfluid velocity of the spinor condensate $\mathbf{v}_s(\mathbf{r})$. Note that in the anisotropic spin-1 case, this mass is, in principle, a tensor, but with only very small nondiagonal components.

Similar to the moment of inertia, we can calculate this mass explicitly for large skyrmions. The result is

$$M=\begin{cases}\dfrac{19\pi}{18\sqrt{2}}\dfrac{\lambda}{a}m, & S=1/2\\[2ex] \dfrac{2\sqrt{2}\pi}{3}\dfrac{\lambda}{a}m, & S=1.\end{cases} \quad (37)$$

The skyrmions thus indeed behave in this respect as ordinary particles. In contrast to Eq. (30), there thus appears no term linear in $\partial\mathbf{u}(t)/\partial t$ in the action $S[\mathbf{u}]$. This is a result of the fact that we have performed all our calculations at zero tem-

perature. In the presence of a normal component, we anticipate the appearance of such a linear term with an imaginary coefficient. This will lead to damping of the center-of-mass motion of the skyrmion. It is interesting to note that if we perform the same analysis for a vortex in a scalar condensate, we find, due to the singular nature of the superfluid velocity field, even at zero temperature an additional term linear in the velocity of the vortex. In a quasi-two-dimensional situation, it is in fact proportional to $\mathbf{u}(t)\times\partial\mathbf{u}(t)/\partial t$. This precisely results in the well-known Euler dynamics of vortices.

V. CONCLUSION

One important conclusion of this paper is that skyrmions in a ferromagnetic Bose-Einstein condensate are energetically unstable. However, we have also shown that the time scale on which the skyrmion decreases may be of the order of, or even larger, than the lifetime of the condensate. It turns out that there are two very different mechanisms for the shrinking of the skyrmion. The first occurs for skyrmions with sizes much larger than the correlation length of the gas. In this case, the shrinking rate is of the order of seconds for realistic experimental parameters. The second case concerns smaller skyrmions with sizes of the order or less than the correlation length of the system. In this case, the shrinking rate is determined by the tunneling rate from the core of the skyrmion to the uniform part of the system. The tunneling takes place through a potential barrier developed by spin deformations. The typical time scale for such a shrinking process is of the order of 10 – 100 s.

Although we have considered a homogeneous discussion, the inclusion of a trap in the system will not change the main conclusions of this paper. The presence of a trap will have the effect that the uniform density n_∞ will be now a position-dependent quantity. Therefore, for our calculations to be valid for a trapped gas, the size of the skyrmion must be much less than the typical length scale for the density gradients of the confined condensate. Thus, the condition $\lambda \ll R$ must be met, where R is the size of a spherical condensate. For typical experimental conditions, we may use the Thomas-Fermi approximation to the size of the condensate [30], which reads $R=\sqrt{2/\pi}(Na/l)^{1/5}l$, where N is the number of atoms in the condensate and $l=\sqrt{\hbar/m\omega_0}$ is the characteristic length of a harmonic trap of frequency ω_0. Scaling R to the correlation length ξ, the former takes the form $R=4N^{1/5}(l/a)^{4/5}$. For a ^{87}Rb condensate with $N=10^6$ atoms and a trap frequency of the order of $2\pi\times 100$ rad/s this gives $R\approx 500$. This gives an estimate for the maximum size of a skyrmion such that the above condition remains valid. For example, our theory for large skyrmions is applicable for the size range of $\lambda=10\xi$ up to say 50ξ.

Another important remark about a confined gas is that skyrmions will tend to move towards the surface of the Bose-Einstein condensate since the density there is lower and thus their energy will be less. Apparently, this leads to a decrease in the shrinking rate since for both large and small skyrmions, the shrinking time is proportional to $1/n_\infty$, see Eq. (21) and the discussion afterwards, and Eq. (29) and the discussion before it. However, our theory for the shrinking rates of skyrmions clearly breaks down on the surface since there the typical length scale for the density gradients due to the trap are of the same order as the correlation length.

Although skyrmion-antiskyrmion pairs can be created by the Kibble mechanism in a temperature quench or by sufficiently shaking up the condensate, a more controlled way of creating a skyrmion may be achieved by using a magnetic-field configuration in which the fictitious magnetic field is always pointing radially outward and its magnitude increases monotonically from zero at the origin to a maximum value for large distances from the origin [31]. Applying this field configuration for such a long time that the spins at large distances have precessed exactly twice around the local magnetic field, creates a single skyrmion. Of course, for a real magnetic field, the above configuration requires the use of magnetic monopoles, but for a fictitious magnetic field, it may be achieved by appropriately tailoring the detuning, the polarization, and the intensity of two pulsed Raman lasers. The required spatial dependence of the detuning may be created experimentally by separating the centers of the magnetic traps for the two spin species along the z axis [4]. Furthermore, the desired behavior of the Rabi frequency may be achieved by making with the first Raman laser two standing waves in the x and y directions that are both polarized perpendicular to the z axis. For the other Raman laser, we only need to require that it produces a traveling wave with a polarization that has a nonzero projection on the z axis, since we want to realize a $\Delta m=0$ transition in this case. In the above geometry the skyrmion is created exactly in the plane where the detuning vanishes and in the nodes of the first Raman laser. Note that since the distance between these nodes is generally much bigger than the correlation length, we create in this manner a large skyrmion that will start to decrease but ultimately self-stabilizes at a smaller size. Once created, the skyrmion may be easily observed by the usual expansion experiments that have recently also been used to observe vortices [32]. Similar as with vortex rings, we then observe an almost complete depletion of the condensate in a ring around the position of the skyrmion.

ACKNOWLEDGMENTS

We would like to thank Eric Cornell and Jan Smit for useful and stimulating discussions. This paper is supported by the Stichting voor Fundamenteel Onderzoek der Materie (FOM), which is financially supported by the Nederlandse Organisatie voor Wetenschappelijk Onderzoek (NWO).

APPENDIX: DETAILS OF THE CALCULATION OF $\langle S_x\rangle$, $\langle S_y\rangle$, $\langle S_z\rangle$, $\zeta^\dagger(\mathbf{r})\nabla\zeta(\mathbf{r})$, AND $|\nabla\zeta|^2(\mathbf{r})$

We start by expanding the exponential operator in Eq. (1), taking into account the simplification expressed in Eq. (3). Inserting the explicit forms of the spin-1/2 and spin-1 matrices given by [33]

$$\mathbf{S}=\begin{cases}\dfrac{1}{2}\begin{pmatrix}0&1\\1&0\end{pmatrix}\hat{\mathbf{x}}+\dfrac{i}{2}\begin{pmatrix}0&-1\\1&0\end{pmatrix}\hat{\mathbf{y}}+\dfrac{1}{2}\begin{pmatrix}1&0\\0&-1\end{pmatrix}\hat{\mathbf{z}}, & S=\dfrac{1}{2}\\ \dfrac{1}{\sqrt{2}}\begin{pmatrix}0&1&0\\1&0&1\\0&1&0\end{pmatrix}\hat{\mathbf{x}}+\dfrac{i}{\sqrt{2}}\begin{pmatrix}0&-1&0\\1&0&-1\\0&1&0\end{pmatrix}\hat{\mathbf{y}}+\begin{pmatrix}1&0&0\\0&0&0\\0&0&-1\end{pmatrix}\hat{\mathbf{z}}, & S=1\end{cases} \tag{A1}$$

and noting that $(\hat{\mathbf{S}}\cdot\hat{\mathbf{r}})^k$equals $\mathbf{S}\cdot\mathbf{r}$ for $k=$odd, and equals $(\mathbf{S}\cdot\hat{\mathbf{r}})^2$ for $k=$even, enables a resuming of the odd and even powers of the exponent separately. As a result, one can put this exponential operator in the following simple form:

$$\exp\left\{-\frac{i}{S}\mathbf{\Omega}(\mathbf{r})\cdot\mathbf{S}\right\}=\exp\left\{-\frac{i}{S}\omega(r)\hat{\mathbf{r}}\cdot\mathbf{S}\right\}=\begin{cases}\mathbf{1}\cos[\omega(r)]-i(\hat{\mathbf{r}}\cdot\mathbf{S})\sin[\omega(r)], & S=\dfrac{1}{2}\\ \mathbf{1}-(\hat{\mathbf{r}}\cdot\mathbf{S})^2[1-\cos(\omega(r))]-i(\hat{\mathbf{r}}\cdot\mathbf{S})\sin[\omega(r)], & S=1,\end{cases} \tag{A2}$$

where **1** is the identity matrix. It is then straightforward to derive the expressions for the important physical quantities such as the average spin components $\langle S_x\rangle=\zeta^\dagger(\mathbf{r})S_x\zeta(\mathbf{r})$, $\langle S_y\rangle$ and $\langle S_z\rangle$, and the superfluid velocity $\mathbf{v}_s=-i\hbar\zeta^\dagger(\mathbf{r})\nabla\zeta(\mathbf{r})/m$. For $S=1/2$ and 1, these quantities take the form

$$\langle S_x\rangle/S=\sin\theta\sin\phi\sin(\omega/S)+\sin(2\theta)\cos(\phi)\sin^2(\omega/2S), \tag{A3}$$

$$\langle S_y\rangle/S=-\sin\theta\cos\phi\sin(\omega/S)+\sin(2\theta)\sin(\phi)\sin^2(\omega/2S), \tag{A4}$$

$$\langle S_z\rangle/S=\cos^2(\theta)+\cos(\omega/S)\sin^2\theta, \tag{A5}$$

and

$$\mathbf{v}_s=\hbar\left[\cos\theta\frac{d\omega}{dr}\hat{\mathbf{r}}-\frac{S}{r}\sin\theta\sin(\omega/S)\hat{\boldsymbol{\theta}}-\frac{2S}{r}\sin\theta\sin^2(\omega/2S)\hat{\boldsymbol{\phi}}\right]. \tag{A6}$$

We may now derive the expression for the spin gradient energy $\hbar^2|\nabla\zeta(\mathbf{r})|^2/2m$ as Eq. (22) shows apart from the constant $\hbar^2/2m$.

[1] D. M. Stamper-Kurn, M. R. Andrews, A. P. Chikkatur, S. Inouye, H.-J. Miesner, J. Stenger, and W. Ketterle, Phys. Rev. Lett. **80**, 2027 (1998).

[2] H.-J. Miesner, D. M. Stamper-Kurn, J. Stenger, S. Inouye, A. P. Chikkatur, and W. Ketterle, Phys. Rev. Lett. **82**, 2228 (1999); D. M. Stamper-Kurn, H.-J. Miesner, A. P. Chikkatur, S. Inouye, J. Stenger, and W. Ketterle, *ibid.* **83**, 661 (1999).

[3] C. J. Myatt, A. E. Burt, R. W. Ghrist, E. A. Cornell, and C. E. Wieman, Phys. Rev. Lett. **78**, 586 (1997).

[4] M. R. Matthews, B. P. Anderson, P. C. Haljan, D. S. Hall, C. E. Wieman, and E. A. Cornell, Phys. Rev. Lett. **83**, 2498 (1999).

[5] J. Stenger S. Inouye, D. M. Stamper-Kurn, H.-J. Miesner, A. P. Chikkatur, and W. Ketterle, Nature (London) **396**, 345 (1999).

[6] D. M. Stamper-Kurn, H.-J. Miesner, A. P. Chikkatur, S. Inouye, J. Stenger, and W. Ketterle, Phys. Rev. Lett. **83**, 661 (1999).

[7] M. R. Matthews, B. P. Anderson, P. C. Haljan, D. S. Hall, M. J. Holland, J. E. Williams, C. E. Wieman, and E. A. Cornell, Phys. Rev. Lett. **83**, 3358 (1999).

[8] T.-L. Ho, Phys. Rev. Lett. **81**, 742 (1998).

[9] T. Ohmi and K. Machida, J. Phys. Soc. Jpn. **67**, 1822 (1998).

[10] C. K. Law, H. Pu, and N. P. Bigelow, Phys. Rev. Lett. **81**, 5257 (1998).

[11] T.-L. Ho and S.-K. Yip, Phys. Rev. Lett. **84**, 4031 (2000).

[12] S.-K. Yip, Phys. Rev. Lett. **83**, 4677 (1999).

[13] S. Tuchiya and S. Kurihara, e-print cond-mat/0101109.

[14] T. H. R. Skyrme, Proc. R. Soc. London, Ser. A **260**, 127 (1961); Nucl. Phys. **31**, 556 (1962).

[15] S. L. Sondhi, A. Karlhede, S .A. Kivelson, and E. H. Rezayi, Phys. Rev. B **47**, 16419 (1993).

[16] H. T. C. Stoof, e-print cond-mat/0002375. The stability analysis in this paper is based on linear-response theory, which unfortunately turns out to be not fully adequate. The nonlinear analysis is presented by U. Al Khawaja and H. T. C. Stoof, Nature (London) **411**, 918 (2001).

[17] G. 't Hooft, Nucl. Phys. B **79**, 276 (1974); A. M. Polyakov, Pis'ma Zh. Éksp. Teor.Fiz. **20**, 450 (1974) [JETP Lett. **20**, 194 (1974)].

[18] H. T. C. Stoof, E. Vliegen, and U. Al Khawaja, e-print cond-mat/0103194.

[19] In principle, this is only true if the inter- and intra-scattering lengths of the two condensate components are equal, which is a good approximation for ^{87}Rb [4].

[20] R. Rajaraman, *Solitons and Instantons* (North-Holland, Amsterdam, 1982).

[21] N. D. Mermin, Rev. Mod. Phys. **51**, 591 (1979).

[22] R. Shankar, J. Phys. (Paris) **38**, 1405 (1977).

[23] D. S. Hall, M. R. Matthews, J. R. Ensher, C. E. Wieman, and

E. A. Cornell, Phys. Rev. Lett. **81**, 1539 (1998).
[24] H. T. C. Stoof, J. Stat. Phys. **87**, 1353 (1997), and references therein.
[25] R. Côté, A. H. MacDonald, L. Brey, H. A. Fertig, S. M. Girvin, and H. T. C. Stoof, Phys. Rev. Lett. **78**, 4825 (1997).
[26] M. Lewenstein and L. You, Phys. Rev. Lett. **77**, 3489 (1996).
[27] H. T. C. Stoof, J. Low Temp. Phys. **114**, 11 (1999).
[28] D. Finkelstein and J. Rubinstein, J. Math. Phys. **9**, 1762 (1968).
[29] F. Wilczek and A. Zee, Phys. Rev. Lett. **51**, 2250 (1983).
[30] G. Baym and C. J. Pethick, Phys. Rev. Lett. **76**, 6 (1996).
[31] J. Ruostekoski and J. Anglin, Phys. Rev. Lett. **86**, 3934 (2001).
[32] K. W. Madison, F. Chevy, W. Wohlleben, and J. Dalibard, Phys. Rev. Lett. **84**, 806 (2000).
[33] See, for example, D. A. Varshalovich, A. N. Moskalev, and V. N. Khersonskii, *Quantum Theory of Angular Momentum* (World Scientific, Singapore, 1988).